Manuscript: "High-Resolution Urban Observation Network for a User-Specific Meteorological Information Service in the Seoul Metropolitan Area, Korea" by Moon-Soo Park et al.

Response to the Anonymous Referee #2

Authors gratefully thank the reviewer for his/her thorough review and valuable comments which contributed to improve the manuscript. Reviewer's all comments except for journal scope are responded. According to the reviewer's suggestion, authors will add two case studies to demonstrate the usefulness and applicability of the UMS-Seoul in Chapter 5. Reviewer's comments are marked in black, while authors' responses are marked in blue.

On journal scope:

⇨ This manuscript had been submitted to AMT by accepting the ACP (Atmospheric Chemistry and Physics) Executive Editor's suggestion. Authors think that this topic is included in the meteorological measurement platform, one of AMT journal's main scopes. Design of an intensive & integrated meteorological observation network for a special purpose is as important as development or improvement of each measurement instrument.

On the absence of case studies or results illustrating the ability of such an integrated system within an urban area to improve now- and fore-casting makes the paper unpublishable in AMT.

⇨ Authors added two case studies using the observation data in Chapter 5 in the revised manuscript. One is for the spatial distribution of surface meteorology and temporal evolution of urban boundary-layer structures during the 3 consecutive days in spring, the other is for finding the road sections vulnerable to road wetness and ice using the surface temperature and status on a roadway obtained by a mobile road weather vehicle.

The following chapter will be added in the revised manuscript.

5. Case Studies

In order to demonstrate the usefulness of UMS-Seoul and applicability to the meteorological information service customized users' demands, two case studies are conducted: One is for the spatial distribution of surface meteorology and the evolution of urban boundary layer structures during the 3 consecutive days in spring, the other is for finding the road sections vulnerable to road wetness and ice using the surface temperature and status on a roadway obtained by a mobile road weather vehicle.

5.1. Case Study I: spring zonal anticyclone event

Surface meteorology and atmospheric boundary layer structures are investigated for the period from 18 to 20 May 2016. During this period, a zonal anticyclone in northern Japan blocks an eastward moving weather system. Thus, a jet stream at 300 hPa level is divided into higher and lower latitude directions over eastern China. As a result, Seoul Metropolitan Area shows a fine weather at the edge of high pressure system. A short-lived and small thermal low pressure system driven by thermal difference between continent and sea is developed in the afternoon and disappears in the evening on 19 and 20 May 2016.

Figure 6 shows a horizontal distribution of air temperature obtained by SKP surface meteorological observation system at 0600 LST, 1200 LST, 1800 LST, and 2400 LST on 18 May 2016. At 0600 LST and 2400 LST when there is no thermal heating, western sites show a relatively high temperature, while eastern sites show a relatively low temperature. On the other hand, at 1200 LST and 1800 LST, eastern sites show a relatively high temperature, while western sites show a relatively low temperature. This temperature difference implies the existence of local circulation such as land and sea breeze, and mountain valley circulation. Urban sites have higher temperature than the surrounding sites throughout the period, which is mainly due to heat capacity difference between the urban and the rural. Temperature difference between two land coves, that is urban heat island effect, becomes stronger during the night.

Figure 7 shows the time series of surface meteorological variables obtained at every 1 minute by a surface energy balance system installed at the Jungnang station for the period from 0000 LST 18 to 2400 LST 20 May 2016. During this period, it was so clear that daily cloud cover was recorded as 0.5/10, 0.0/10, and 0.6/10 in 18, 19, and 20 May 2016, respectively. Air pressure minimum is occurred at around 1500-1800 LST every day (Figs. 7a, b, d, e), which is accompanied by a wind speed, direction, and vapor pressure change. That is to say, after low air pressure passes the station, wind direction is abruptly changed to northwesterly, air temperature drops down by 1.8 ℃ (3.5 ℃), and

vapor pressure jumps up by 2.6 hPa (8.0 hPa) on 19 (20) May. Diurnal variation of wind speed and direction shows that the station is affected by local circulations: northeasterly winds are dominant at night, while other directional winds are dominant in a day (Figs. 7c and d). Net radiation is negative at night and positive during the day, the variation of which shows that there are few clouds in this period except for in the afternoon 20 May (Fig. 7f).

Figure 8 shows the backscattering coefficient observed by a ceilometer and vertical profile of wind observed by a wind lidar at the Jungnang station for the period from 0000 LST 18 to 2400 LST 20 May 2016. Atmospheric boundary-layer structures defined by a backscattering coefficient are perfectly coincident with those defined by a wind: (1) Backscattering coefficient shows that there are two distinct layers before 1000 LST 18 May; the lower layer with a maximum height of 400 m contains thick backscattering aerosols, while the upper layer has less dense to 1.2 km. Wind profile also shows that two layers have different origins: Easterly winds are dominant at lower layer, while westerly winds are dominant at upper layer; (2) Convective atmospheric boundary layer defined by a backscattering coefficient evolves during the day on 3 consecutive days. Correspondingly, winds become irregular throughout the same layer; (3) Residual layer with a high backscattering coefficient around 2 km high at night move downward slowly to the next morning time, and combine with the evolving convective boundary layer at noon in 19 May. Southerly winds are in upper residual layer, while northerly or north-easterly winds are in lower stable boundary layer; High backscattering coefficient zones at from 500 m to 1500 m high on 0300 to 09 LST and at height than 1000 m on near 1800 LST 20 May are exactly corresponded to the wind convergence zone. Potential temperature and mixing ratio profiles obtained by a microwave radiometer also supports the similar atmospheric boundary-layer structures (Fig. 9). To be concluded, surface meteorology and vertical profiles of meteorological variables observed from the UMS-Seoul will be very helpful to produce the high-quality and high-resolution meteorological field in the SMA.

5.2. Case study II: mobile road weather vehicle

Figure 10 shows an example of the road surface temperature service on a roadway route in Seoul Metropolitan Area observed by a mobile road weather vehicle with the road material, structure and elevation for the period from 1000 to 1440 LST on 2 December 2016. The road material is classified as asphalt (72.2 %) and concrete (27.8 %), while road structure is classified as over-ground (86.2 %), bridge (10.4 %), underpass (0.6 %), and tunnel (2.8 %) roads (Table 7). The road elevation is observed by the global positioning system sensor. The surface temperature is found to be related to the road elevation, surface material, road structure, sky-view, and horizontal distribution of surface land

use. The surface temperature over concrete-road is lower than that over asphalt-road due to the difference of albedo and diffusivity (Fig. 11). While that over bridge is higher than that over an over-ground due to the difference of thermal heat capacity and heat transfer processes. Using these data, the roadway sections vulnerable to road wetness and icing on the highways and major principal roads can be determined (Fig. 12). These vulnerabilities will be applicable to give the alarm or advisory to drivers. Also, these data will be applicable to improve the road surface temperature and status prediction system (Park et al., 2014).

Table 7 Coverage fraction for road material and structure on the roadway route observed during 1000 and 1440 LST on 2 December 2016.

Material	Structure	Coverage (%)
Asphalt	Over-ground (AG)	67.18
	Bridge (AB)	3.77
	Underpass (AU)	0.57
	Tunnel (AT)	0.67
Concrete	Over-ground (CG)	19.04
	Bridge (CB)	6.59
	Underpass (CU)	0.00
	Tunnel (CT)	2.18
Total		100.00

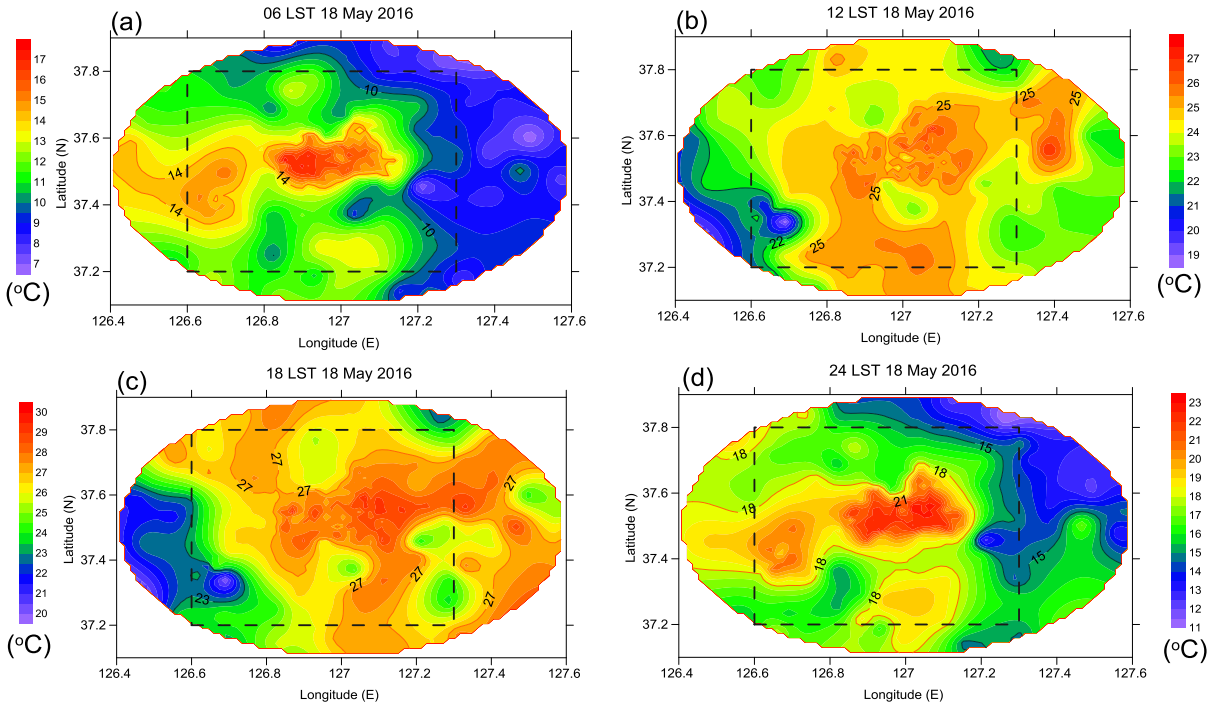

Figure 6: Horizontal distribution of air temperature obtained by SKP surface meteorological observation system at (a) 0600 LST, (b) 1200 LST, (c) 1800 LST, and (d) 2400 LST 18 May 2016 in the Seoul Metropolitan Area. Dotted rectangle denotes the high-populated region in Figure 1b.

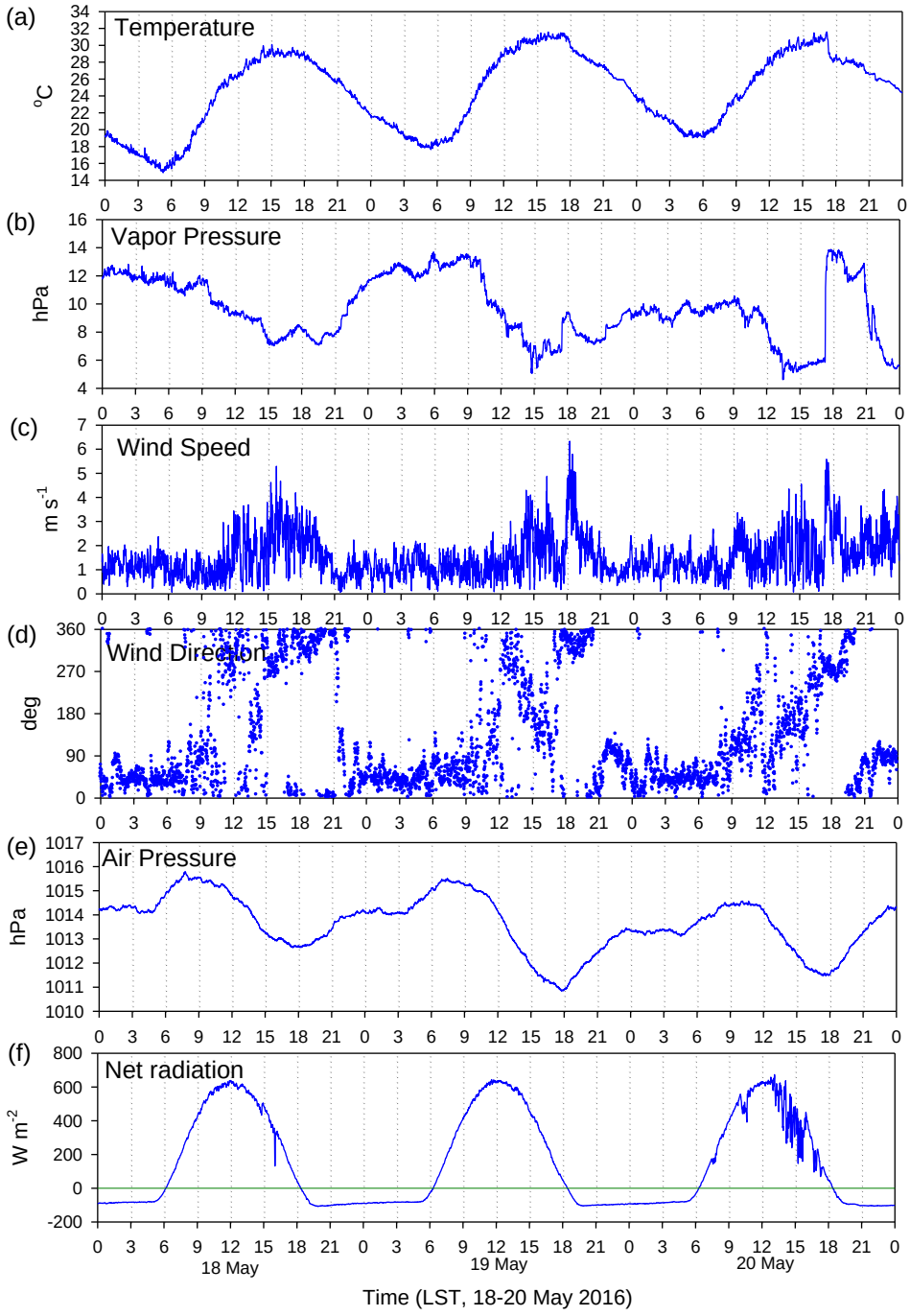

Figure 7: Time series of (a) air temperature, (b) vapor pressure, (c) wind speed, (d) wind direction, (e) air pressure, and (f) net radiation observed at the Jungnang station for the period from 18 to 20 May 2016.

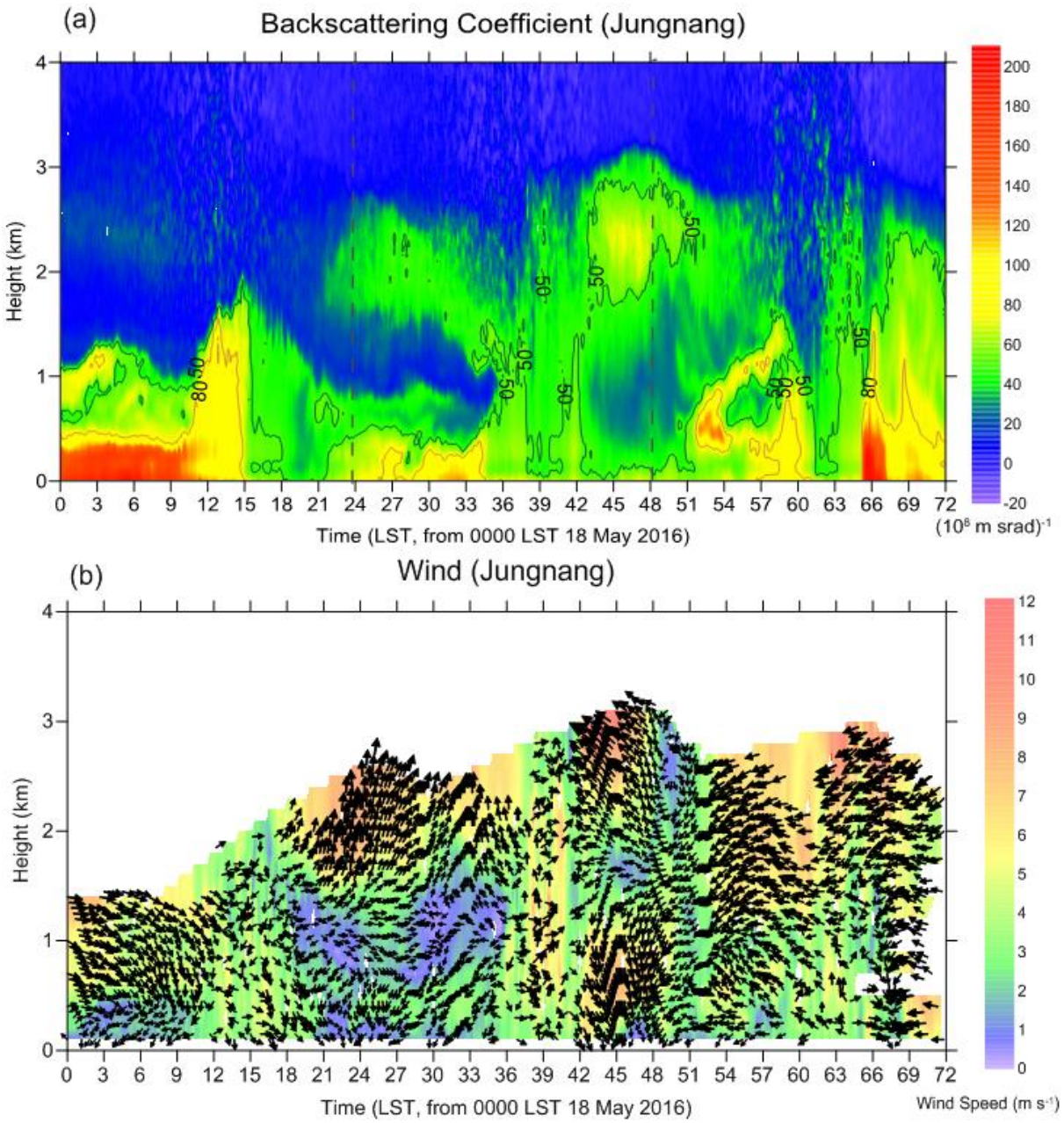

Figure 8: Time-height cross sections of (a) backscattering coefficient obtained by a ceilometer, and (b) wind speed and direction obtained by a wind lidar at the Jungnang station for the period from 0000 LST 18 to 0000 LST 21 2016.

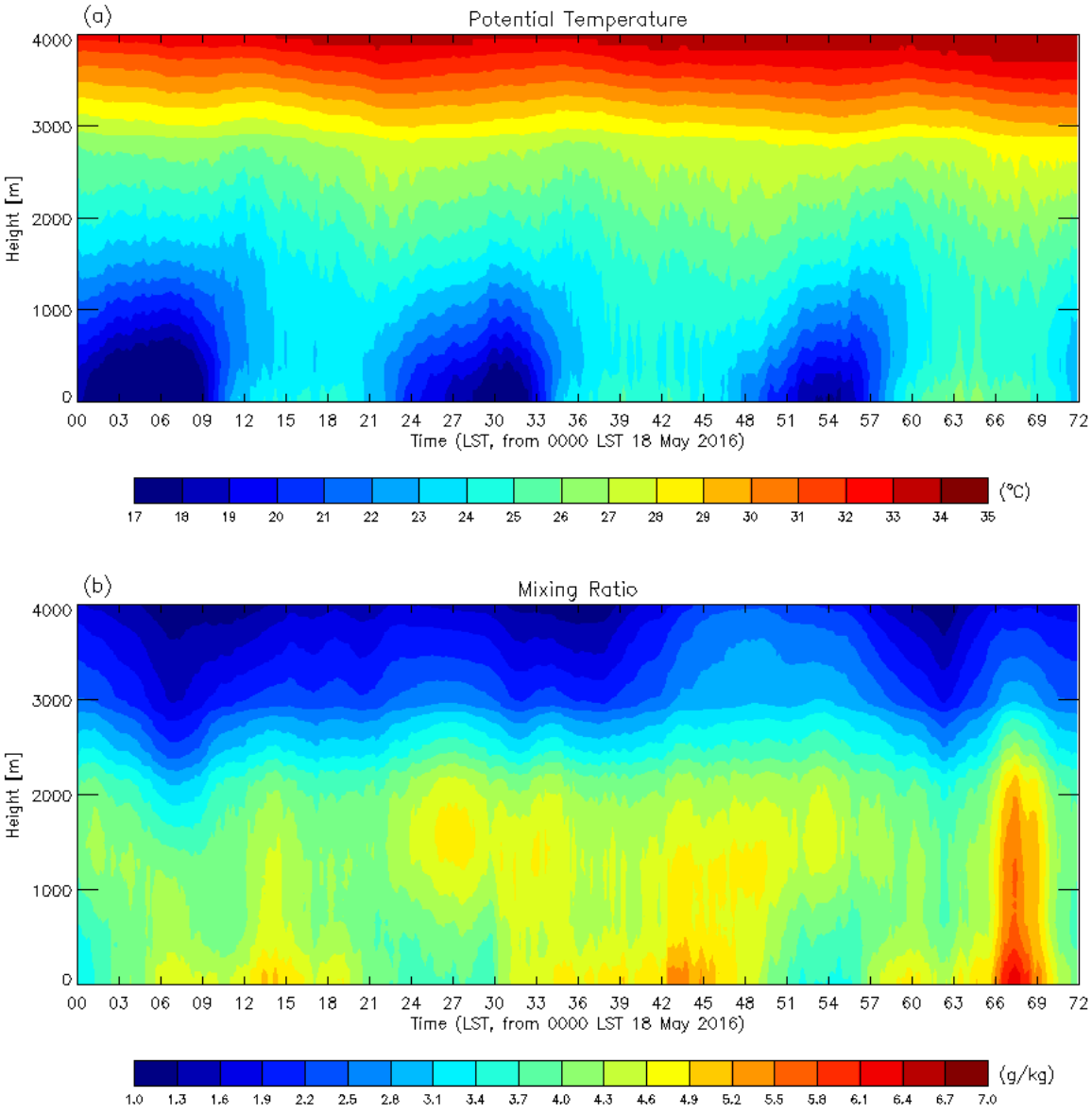

Figure 9: Time-height cross sections of (a) (a) potential temperature and (b) mixing ratio obtained by a microwave radiometer at the Jungnang station for the period from 0000 LST 18 to 0000 LST 21 May 2016.

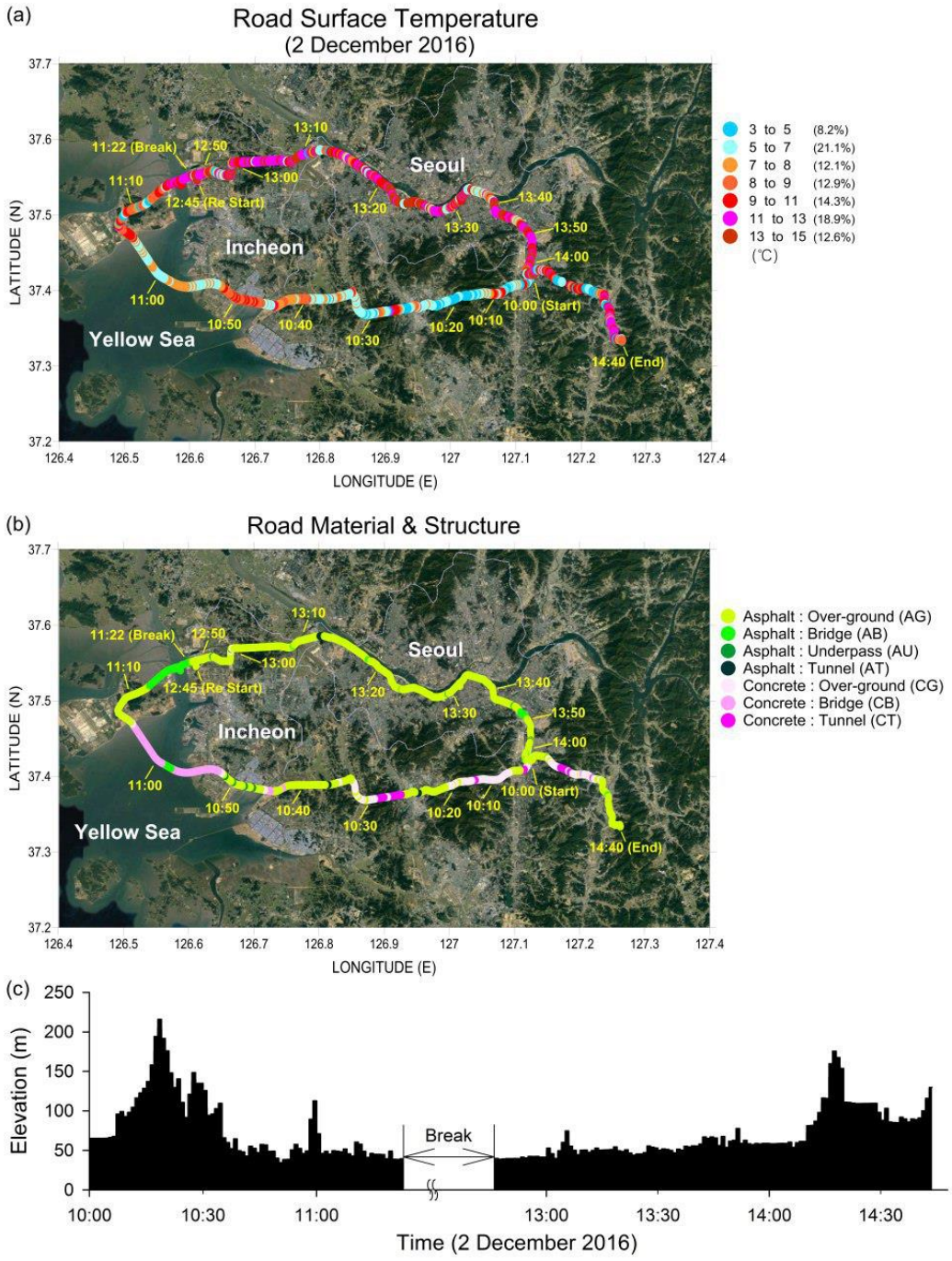

Figure 10: (a) Road surface temperature, (b) road surface material and structure, and (c) elevation on the roadway obtained by a mobile road weather vehicle in the Seoul Metropolitan Area for the period from 1000 LST to 1440 LST 2 December 2016.

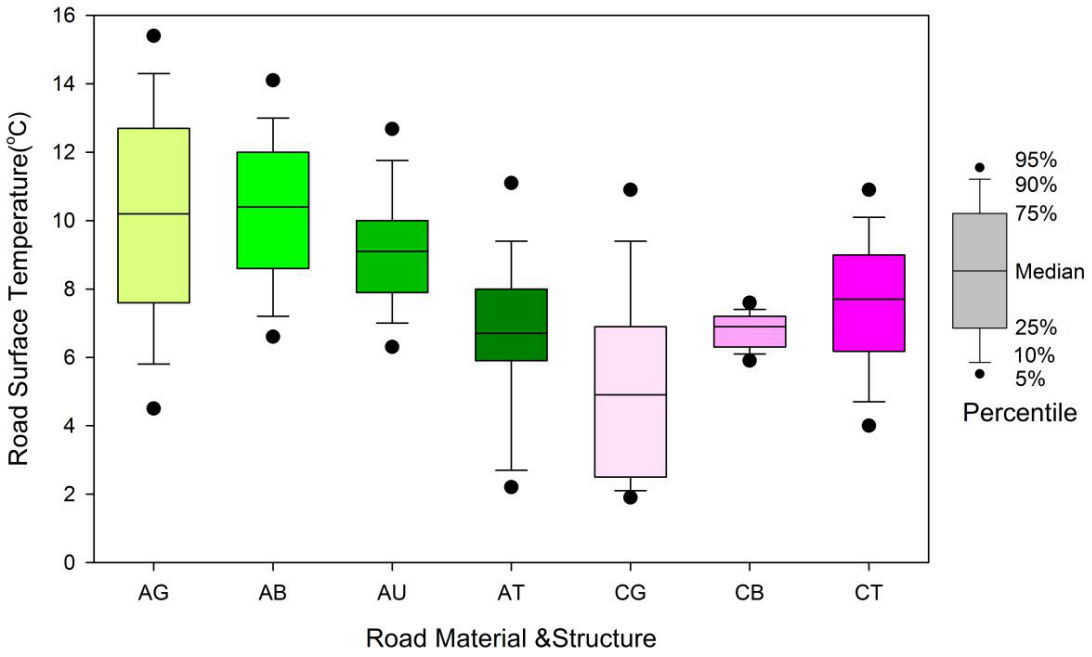

Figure 11: Boxplot of observed road surface temperatures according to road material and structure on the roadway obtained by a mobile road weather vehicle in the Seoul Metropolitan Area for the period from 1000 LST to 1440 LST 2 December 2016. First character stands for road material type: A does for Asphalt, C for concrete. Second character denotes road structure type: G for over-ground, B for bridge, U for underpass, and T for tunnel.

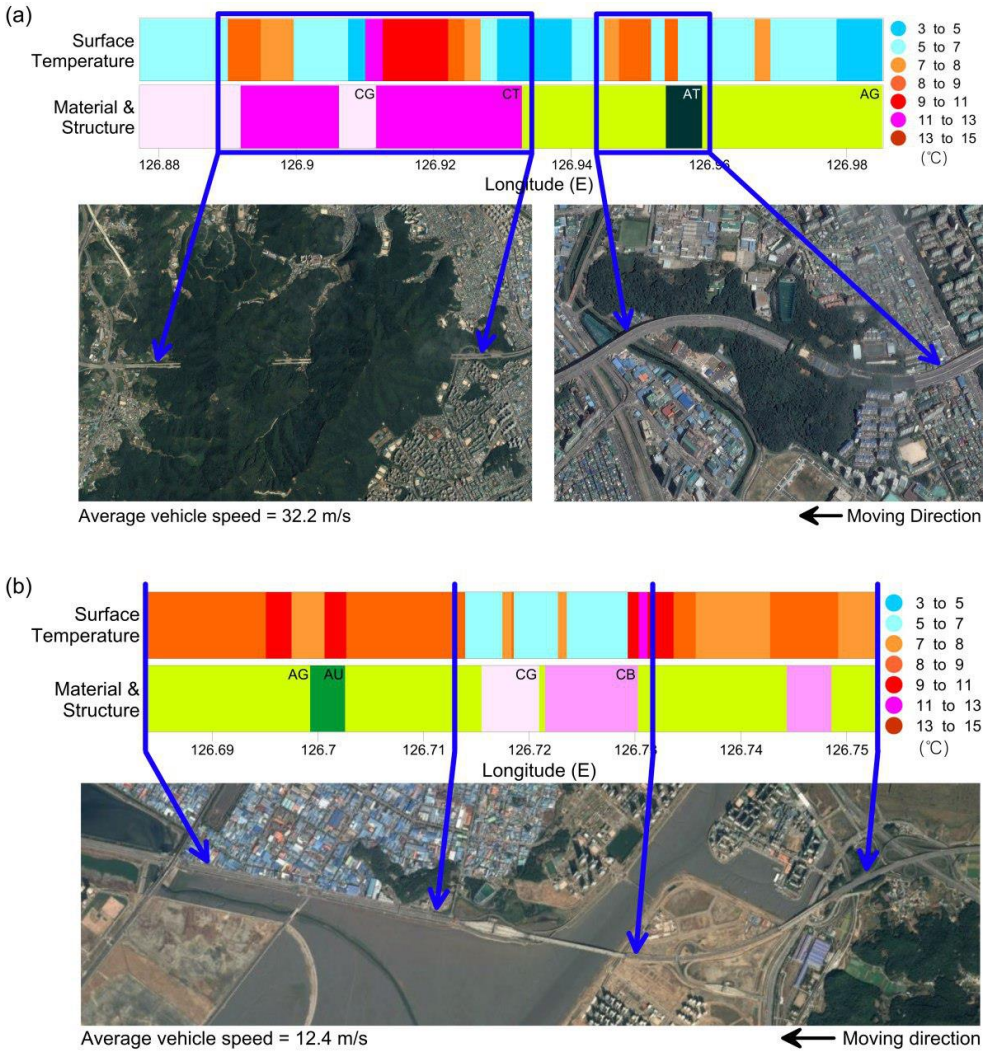

Figure 12: Detailed surface temperature and material & structure with a satellite image at road sections (a) from 126.88E to 126.98E and (b) from 126.68E to 126.76E in Figure 10. First character stands for road material type: A does for Asphalt, C for concrete. Second character denotes road structure type: G for over-ground, B for bridge, U for underpass, and T for tunnel.